Diversified repertoire of phage defenses in *Klebsiella pneumoniae*: Bi-directional steering effects impacting antibiotic susceptibility

Sue C. Nang[1], Jing Lu[1], Heidi H. Yu[1], Hasini Wickremasinghe[1], Mohammad A. K. Azad[1], Meiling Han[1], Jinxin Zhao[1], Gauri Rao[2], Phillip J. Bergen[1], Tony Velkov[1], Norelle Sherry[3], David T. McCarthy[4], Saima Aslam[5], Robert T. Schooley[5], Benjamin P. Howden[3], Jeremy J. Barr[6], Yan Zhu[1], Jian Li[1*]

[1]Biomedicine Discovery Institute, Infection Program, Department of Microbiology, Monash University, Clayton, Victoria, Australia.

[2]Division of Pharmacotherapy and Experimental Therapeutics, Eshelman School of Pharmacy, University of North Carolina, Chapel Hill, North Carolina, USA.

[3]Microbiological Diagnostic Unit Public Health Laboratory, Department of Microbiology and Immunology, The University of Melbourne at The Peter Doherty Institute for Infection and Immunity, Melbourne, Victoria, Australia.

[4]Department of Civil Engineering, Monash University, Clayton, Victoria, Australia.

[5]Division of Infectious Diseases and Global Public Health, Department of Medicine, University of California San Diego, La Jolla, California, USA.

[6]School of Biological Sciences, Monash University, Clayton, Victoria, Australia.

*Corresponding author. Email: jian.li@monash.edu

Abstract

Phage therapy is a promising alternative treatment for multidrug-resistant bacterial infections. Unfortunately, phage resistance represents a major barrier hindering the clinical utility. Mechanistic insights into bacterial phage defense mechanisms are critical to optimize phages therapy. Here, we discovered a repertoire of phage resistance mechanisms in a model strain *Klebsiella pneumoniae* MKP103, including the disruption of phage binding site (*fhuA*::Tn and *tonB*::Tn), extension of phage latent period (*mnmE*::Tn and *rpoN*::Tn) and increased mutation frequency (*mutS*::Tn and *mutL*::Tn). Different from the prevailing view that phage resistance re-sensitizes antibiotic-resistant bacteria, we demonstrated a bi-directional steering effect on antibiotic susceptibility. Specifically, it was uncovered that, while *rpoN*::Tn became more susceptible to colistin, *mutS*::Tn and *mutL*::Tn caused increased resistance to rifampicin and the last-line colistin. Our findings highlight the diversified strategies utilized by *K. pneumoniae* to overcome phage infection. Overall, mechanism-guided phage steering represents a vital strategy to maximize the success of phage therapy.

35 **Introduction**

36 Bacteriophages (phages) are viruses that specifically target bacteria[1, 2]. The earliest
37 recorded therapeutic practice of phages for the treatment of bacterial infections took place
38 almost a century ago[3, 4, 5], prior to the discovery of penicillin[6]. Unfortunately, as the golden
39 age of antibiotic was on the rise, phage therapy was abandoned mainly due to technical and
40 logistical hurdles[3]. In recent times, the 'perfect storm' of widespread antimicrobial resistance
41 (AMR) combined with the sparse antibiotic development pipeline has dramatically reduced
42 the antibiotic armamentarium available to physicians for treating multidrug-resistant (MDR)
43 infections[7, 8]. Of particular concern are the ESKAPE pathogens which 'escape' the antibacterial
44 effects of many antibiotics through a wide range of resistance mechanisms[9, 10]. With the dawn
45 of a post-antibiotic era rapidly emerging, the World Health Organization (WHO) and the
46 Centers for Disease Control and Prevention (CDC) have declared AMR as a major global health
47 threat[11, 12]. Clearly, alternative antimicrobial therapies are urgently required and therefore,
48 significant interest has risen in the use of phages for MDR bacterial infections[3, 4, 13]. To date,
49 the clinical utility of phages has been hampered by a poor knowledge base on their biology,
50 resistance mechanisms and combination use with antibiotics[3]. A concept receiving significant
51 favorable attention recently in the AMR field is 'phage steering' which involves the use of
52 phages to kill susceptible bacterial cells while re-sensitizing the remaining phage-resistant
53 bacterial population to antibiotics[14, 15]. The utility of phage steering lies in the prospect of
54 eliminating the entire bacterial populations using phage-antibiotic combinations[14, 15];
55 however, the intricacies and limitations of phage steering have yet to be explored. Here, we
56 discovered an unprecedented bi-directional phage steering effect with decreased and
57 increased antibiotic susceptibility associated with the repertoire of phage resistance
58 mechanisms.

59 **Results**

60 *Phage resistome screening reveals involvement of diverse genes*

61 Most phage resistance studies in the literature have relied on the use of a population-
62 based whole-genome sequencing method, which often limits the detection of phage
63 resistance mechanisms to those associated with phage binding sites such as the capsule[15, 16],
64 lipopolysaccharide (LPS) and outer membrane protein components[16, 17, 18]. Utilizing a strictly
65 lytic *Siphoviridae* phage pKMKP103_1 (**Fig. 1**), we conducted a genome-wide resistome study
66 by investigating the susceptibility of individual transposon mutants of *K. pneumoniae*
67 MKP103[19]. Screening of phage resistome identified six genes, *rpoN*, *mutS*, *mutL*, *mnmE*, *fhuA*
68 and *tonB*, in *K. pneumoniae* MKP103 that are associated with effective pKMKP103_1 infection
69 (**Fig. 2a and Supplementary Table 1**). Subsequently, we proceeded to confirm the phage
70 susceptibility of these candidate transposon mutants by evaluating: (i) the ability of
71 pKMKP103_1 to form clear plaques on soft agar containing the respective mutants (**Fig. 2b**),
72 and (ii) the killing kinetic profiles of pKMKP103_1 against the respective mutants in broth (**Fig.
73 2c**). Against *fhuA*::Tn and *tonB*::Tn, pKMKP103_1 did not show any lysis zone on agar plates
74 (**Fig. 2b**) nor killing in broth (**Fig. 2c**), potentially attributed by the inability of pKMKP103_1 to
75 infect these mutants. The efficiency of plating (EOP) of pKMKP103_1 on *mnmE*::Tn was
76 reduced (**Fig. 2b**), showing that the ability of pKMKP103_1 to form plaque on this mutant was
77 restricted. A reduced bacterial killing was also illustrated with *mnmE*::Tn over the initial 4 h
78 (**Fig. 2c**). Interestingly, although the EOP of pKMKP103_1 on *rpoN*::Tn was unaffected (**Fig.
79 2b**), no bacterial reduction was observed in the time-kill studies over 24 h (**Fig. 2c**). With
80 *mutS*::Tn and *mutL*::Tn, the EOP of pKMKP103_1 was similar to the WT (**Fig. 2b**); however, a
81 weaker initial killing activity was evident in broth (**Fig. 2c**).

82

83 *Phage resistance is associated with multiple mechanisms*

84 As different phage susceptibility profiles were demonstrated by the aforementioned
85 mutants, we proceeded to investigate the mechanisms causing these differential degrees of
86 resistance. The adsorption of pKMKP103_1 to the bacterial surface of *fhuA*::Tn and *tonB*::Tn
87 was inhibited (**Fig. 3a–b**). FhuA gating loop has been previously reported to be the binding
88 site for phages T1, T5 and Φ80 in *Escherichia coli*[21], irrespective of conformational changes
89 induced by TonB[22, 23]. In contrary to these earlier studies, pKMKP103_1 in our study
90 potentially have a higher specificity for its binding to *K. pneumoniae* MKP103 as the disruption
91 of either *fhuA* or *tonB* alone was sufficient to prevent the binding of pKMKP103_1 to this
92 strain.

93 As the adsorption of pKMKP103_1 onto the bacterial surface of *mnmE*::Tn, *rpoN*::Tn,
94 *mutS*::Tn and *mutL*::Tn was unaffected (**Fig. 3b**), we subsequently examined the impact for
95 the disruption of these genes on the lytic lifecycle of pKMKP103_1 by examining the phage
96 one-step growth profiles with these respective mutants. With *mutS*::Tn and *mutL*::Tn as the
97 host strains, similar one-step growth profiles of pKMKP103_1 to that observed with the WT
98 were demonstrated (**Fig. 3c**). Interestingly, a longer latent period (40 min) compared to the
99 WT (30 min) was displayed by pKMKP103_1 when *mnmE*::Tn and *rpoN*::Tn were employed as
100 the host strains; however, there were no substantial differences in the burst size (**Fig. 3c**). To
101 the best of our knowledge, this study is the first to identify the association of phage resistance
102 with disrupted bacterial *mnmE*, in which this gene encodes a GTPase involved in the
103 modification of tRNA wobble uridine[24]. Our results indicate that mutation of *mnmE* can
104 substantially delay phage replication; however, the exact mechanism warrants further
105 investigation. For RpoN, an RNA polymerase factor sigma-54 which regulates the transcription
106 of genes across diverse cellular functions[25, 26, 27, 28], a previous study reported its association

107 with phage resistance in *Pseudomonas aeruginosa*[29]. With the diverse regulatory roles played
108 by RpoN, the specific mechanism for its association with phage infection is unknown. Phage
109 resistance due to *rpoN* mutation was postulated to be associated with changes in LPS
110 structure as RpoN has been well known to regulate LPS biosynthetic pathway[29, 30]. We
111 conducted lipid A profiling and revealed that, compared to the WT, there were decreased
112 abundance of L-Ara4N-modified lipid A and increased abundance of 2-hydroxymyristate lipid
113 A in *rpoN*::Tn (**Fig. 4a**), confirming the regulatory role of RpoN on the lipid A modification
114 pathways in *K. pneumoniae* MKP103. Further examinations on the transposon mutants of
115 *arnT* (required for L-Ara4N modification of lipid A) and *lpxO* (required for 2-hydroxylation of
116 the myristate group on lipid A) demonstrated that the infectivity of pKMKP103_1 on these
117 mutants was similar to that on the WT. Our result shows that these lipid A species are not
118 involved in pKMKP103_1 infection.

119 Notably, we demonstrate for the first time that the rapid emergence of phage
120 resistance can occur in *K. pneumoniae* with disrupted *mutS* and *mutL*. Bacterial isolates with
121 interrupted *mutS* and *mutL* are commonly known as hypermutators[31, 32, 33, 34] and are
122 frequently associated with antibiotic resistance[35]. Compared to the WT, a significant increase
123 in mutation frequency to pKMKP103_1 was discovered with *mutS*::Tn and *mutL*::Tn (**Fig. 3d**).
124 Furthermore, complementation of *mutL* fully restored the mutation frequency of *mutL*::Tn.
125 While for *mutS*::Tn, a reduced mutation frequency was observed following complementation;
126 however, it did not reach the WT level. Altogether, these findings highlight the important role
127 of the DNA mismatch repair system in preventing the rapid emergence of resistance during
128 phage therapy. Different from our result in *K. pneumoniae* where MutL played a preventive
129 role against phage resistance, MutL caused phage resistance in *P. aeruginosa* by promoting
130 the deletion of a large chromosomal fragment containing *galU*, leading to a lack of *O*-antigen

131 (the binding site for phage PaoP5)[36]. Taken together, this highlights the complexity of the
132 functionality of this DNA mismatch repair system in relation to phage resistance among
133 different bacterial species.
134
135 *Bi-directional steering effects on polymyxin susceptibility in phage-resistant mutants*
136 In the contemporary literature, 'phage steering' has been portraited as a promising
137 antibacterial strategy, having the potential to eliminate the entire bacterial population with
138 phage-antibiotic combination[14, 15, 37]. There have been reports on increased susceptibility to
139 beta-lactams of a phage-resistant *A. baumannii* due to capsule loss[15] and an improved
140 susceptibility of *P. aeruginosa* to erythromycin, tetracycline and ciprofloxacin, following the
141 exposure to phage OMKO1 (known to interact with efflux pumps)[14]. In the case of *K.*
142 *pneumoniae*, the loss of the multidrug-resistance phenotype was observed following the
143 emergence of phage resistance, caused by the loss of antimicrobial resistance genes [bla_{CTX-M},
144 *ant(3")*, *sul2*, *folA*, *mph(E)/mph(G)*] on a plasmid[37]. Hereby, we examined whether the phage
145 resistome repertoire identified in this study would affect the antibiotic susceptibility of
146 *K. pneumoniae* MKP103 (**Fig. 4b and Supplementary Table 2**). For the first time, we revealed
147 a bi-directional antibiotic susceptibility effect caused by different bacterial mechanisms of
148 resistance to a single phage. In comparison to the WT (rifampicin minimum inhibitory
149 concentration [MIC]=64 mg/L; colistin MIC=32 mg/L), phage-resistant *K. pneumoniae* mutants
150 with the hypermutator phenotype (*mutS*::Tn and *mutL*::Tn) exhibited increased resistance to
151 rifampicin (MIC>128 mg/L) and the last-line antibiotic colistin (MIC=128 mg/L); whereas
152 *rpoN*::Tn showed decreased resistance to colistin (MIC=4 mg/L; **Fig. 4b**). The
153 complementation of mutants with the respective WT genes restored the antibiotic
154 susceptibilities to the WT levels, confirming that the disruption of these genes was indeed

155 directly associated with the change in bacterial susceptibility to rifampicin and/or colistin in
156 *K. pneumoniae* MKP103 (**Fig. 4b**). Moreover, we conducted population analysis profiles (PAPs)
157 of colistin with *mutS*::Tn, *mutL*::Tn and *rpoN*::Tn to further examine the susceptibility change.
158 PAPs revealed an ~100-fold increase in the subpopulation of *mutS*::Tn and *mutL*::Tn on
159 Mueller Hinton (MH) agar containing 128 mg/L colistin, when compared to the WT (**Fig. 4c**).
160 In the case of *rpoN*::Tn, compared to the WT, there was ~1,000-fold reduction in the
161 subpopulation growing on MH agar containing 16 and 32 mg/L colistin and ~100-fold
162 reduction in the subpopulation growing on MH agar containing 64 mg/L colistin (**Fig. 4c**). The
163 reduced abundance of L-Ara4N-modified lipid A in *rpoN*::Tn (**Fig. 4a**) explained the reduced
164 colistin resistance in this mutant.
165
166 In conclusion, the bi-directional steering effects of phage therapy we discovered here
167 (**Fig. 5**) highlight the need for extra caution with phage steering and phage-antibiotic
168 combination therapy. Although multiple recent studies have demonstrated the potential of
169 phage steering as a promising approach to restore antibiotic susceptibility in bacteria[14, 15, 37],
170 our findings stress that the importance of understanding the underlying mechanisms.
171 Systematic mechanistic investigations on phage resistance and phage steering are required
172 to facilitate efficacious phage therapy in patients and minimize the risk for the emergence of
173 antibiotic resistance.
174

175 **Methods**

176

177 *Bacteria and phage*

178 *K. pneumoniae* MKP103 and the transposon library mutants were used in this study[19].
179 Transposon mutants were selected from Luria Bertani (LB) agar containing 100 mg/L
180 chloramphenicol during initial isolation[19]. All experiments were conducted in nutrient broth
181 (Oxoid) unless stated otherwise. Phage pKMKP103_1 was isolated from sewage water
182 obtained from a water treatment plant in Melbourne (Victoria, Australia) with *K. pneumoniae*
183 MKP103 as the host strain. The isolation, purification and amplification of phages were
184 conducted according to the Phage on Tap protocol[38].

185

186 *Phage DNA extraction and genome sequencing*

187 Phage pKMKP103_1 was propagated to a titer of ~10^{10} pfu/mL using the plate lysate
188 method[38] and DNA was extracted using the phenol-chloroform method[39]. Briefly, the phage
189 was treated with DNase I (Qiagen) and RNase A (Roche) to remove exogenous bacterial DNA
190 and RNA prior to the addition of sodium dodecyl sulphate and proteinase K to release the
191 DNA from phage particles. Phage DNA was isolated using phenol-chloroform followed by
192 precipitation with isopropanol and 3.0 M sodium acetate (pH 5.2). After two washes with 70%
193 ethanol, DNA was resuspended in DNase-free water. The quality and quantity of DNA were
194 determined using Nanodrop. Sequencing was performed by Genewiz (Suzhou, China) on the
195 Illumina HiSeq. Raw reads (150 bp paired-end) were trimmed and used for *de novo* assembly
196 using SPAdes 3.15.3[40]. Annotation was performed using RAST[41] and PHASTER[42], and
197 hypothetical proteins were further annotated using Blastp (≥90% coverage and ≥80%

198 similarity). Blast Ring Image Generator (BRIG) was used to create a representative
199 visualization of the phage pKMKP103_1 genome[20].
200
201 *Transmission electron microscopy*
202 High purity pKMKP103_1 was prepared using the cesium chloride gradient method[43].
203 For TEM imaging, 5 µL of the phage solution was applied to a glow-discharged carbon-coated
204 copper grid and stained with 1% uranyl acetate. Imaging was conducted on a JEOL JEM-
205 1400Plus TEM (Ramaciotti Centre for Cryo-Electron Microscopy, Monash University). ImageJ
206 (https://imagej.nih.gov/ij/) was used for visualizing and measuring the dimensions of the
207 phage.
208
209 *Genome-wide transposon screening of phage-resistant mutants*
210 The transposon mutant library of *K. pneumoniae* MKP103[19] was utilized for the
211 screening of phage pKMKP103_1-resistant mutants. A 96-pin replicator was used to inoculate
212 the mutants into 96-well plates (each well containing 200 µL of nutrient broth) which were
213 then incubated at 37°C for 18 h to reach ~10^9 cfu/mL. A 10-fold dilution (20 µL in 180 µL) was
214 conducted twice using 96-well plates to achieve a starting bacterial inoculum of ~10^7 cfu/mL.
215 Phage pKMKP103_1 was added to the wells to achieve a multiplicity of infection (MOI) of 1
216 (~10^7 pfu/mL). *K. pneumoniae* MKP103 (WT) was included as the control in each round of the
217 screening experiments. OD_{600nm} was measured at 8 and 10 h with a SPECTROstar® Nano
218 Microplate Reader (BMG Labtech); these time-points were chosen based on preliminary
219 experiments conducted with the WT strain which demonstrated an increase in OD_{600nm} after
220 10 h of incubation. Consequently, mutants with greater OD_{600nm} in comparison to the WT at
221 8 and/or 10 h (OD_{600nm} ≥0.12) were potential resistant mutants. This transposon mutant

222 library consists of 1 to 6 individual transposon-inserted mutant(s) of each non-essential
223 gene[19]. The screening process was narrowed to the genes of which ≥2 individual transposon
224 mutants were identified; additionally, sole transposon mutants were also included to prevent
225 missing out of any potential candidates. With these selected mutants, turbidimetric assays
226 were conducted in three biological replicates followed by time-kill analyses to confirm the
227 phage-resistant phenotype.
228
229 *Complementation of mutants*
230 Sanger sequencing was first conducted to confirm that the mutants contain the
231 transposon at the indicated site (**Supplementary Table 3**). To complement the gene into the
232 respective transposon mutant, the gene was amplified by PCR from the WT strain
233 (**Supplementary Table 3**). PCR products and pBBR1MCS-5[44] (carrying the gentamicin
234 resistance cassette) were digested over 4 h with the restriction enzymes targeting the
235 relevant restriction sites (**Supplementary Table 3**). Following clean-up of the digested
236 products, the PCR product and pBBR1MCS-5 were ligated overnight at 4°C. The ligation
237 mixture was then transformed into chemically competent *Escherichia coli* DH5α and plated
238 on LB agar containing 20 mg/L gentamicin. Colony PCR was conducted to identify the colonies
239 with successful ligation of the gene of interest to pBBR1MCS-5. The plasmid was extracted
240 from *E. coli* DH5α using a QIAprep® Miniprep Kit and Sanger sequencing was conducted to
241 confirm the correct ligation. The complemented plasmids were electroporated into the
242 electrocompetent transposon mutants of the respective gene. An empty pBBR1MCS-5 vector
243 (p_{Vector}) was also electroporated into WT and all mutants as control strains for the experiments
244 to exclude vector effects. Successful transformation was confirmed with the growth of
245 colonies on LB agar containing 20 mg/L gentamicin, followed by PCR.

246

247 Turbidimetric assays

248 *K. pneumoniae* strains were grown in nutrient broth at 37°C with shaking (200 rpm)
249 for 18 h. The overnight bacterial culture was inoculated in fresh nutrient broth (1:100 dilution)
250 and incubated until log-phase with an OD_{600nm} of 0.5 (equivalent to ~10^8 cfu/mL). The culture
251 was then diluted 1:10 with fresh nutrient broth to reach a final inoculum of ~10^7 cfu/mL.
252 Phage pKMKP103_1 was added at an MOI of 1 (final titer of ~10^7 pfu/mL) or 10 (final titer of
253 ~10^8 pfu/mL). Continuous OD_{600nm} readings were taken hourly for 20 h with a SPECTROstar®
254 Nano Microplate Reader (BMG Labtech).

255

256 *Time-kill kinetics*

257 *K. pneumoniae* strains were grown in nutrient broth at 37°C with shaking (200 rpm)
258 for 18 h. The overnight bacterial culture was inoculated in fresh nutrient broth (1:100 dilution)
259 and incubated until log-phase with an OD_{600nm} of 0.5 (equivalent to ~10^8 cfu/mL). The culture
260 was then diluted 1:10 with fresh nutrient broth to reach a final inoculum of ~10^7 cfu/mL.
261 Phage pKMKP103_1 was added at an MOI of 10 (final titer of ~10^8 pfu/mL). For mutants
262 carrying the empty vector and complemented strains, 5 mg/L gentamicin was added as the
263 selection pressure to maintain the plasmid throughout the experiment. An aliquot of 200 µL
264 of culture was collected at 0, 1, 2, 4 and 24 h, centrifuged at 10,000 × *g*, and the bacterial
265 pellet was resuspended in an equal volume of 0.9% NaCl. Following 10-fold dilutions with 0.9%
266 NaCl, 10-µL spots were plated on nutrient agar for viable counting.

267

268 *Efficiency of plating (EOP)*

269 The EOP was conducted to measure the lysis ability of the phage[45]. An overnight

270 bacterial culture was prepared as described above, with 100 µL of the culture subsequently
271 mixed with 4 mL soft agar and poured onto a nutrient agar plate to form double-layered agar
272 containing bacteria. Phage pKMKP103_1 at 10^9 pfu/mL (determined with the WT) was
273 subjected to a series of 10-fold dilutions using SM buffer (50 mM Tris-HCl, 100 mM NaCl, 8
274 mM $MgSO_4$, pH7.4) and plated onto the double-layered agar as 10-µL spots. Plates were then
275 incubated overnight at 37°C before enumeration of visible plaque.
276
277 *Phage adsorption assay*
278 *K. pneumoniae* was grown to log-phase as described above and diluted to ~10^7 cfu/mL
279 (final volume of 1 mL). Phage pKMKP103_1 was then added to reach a final titer of 2.5×10^4
280 pfu/mL (MOI of 0.0025). At 2-, 4- and 10-min following co-incubation, 100-µL was collected
281 and centrifuged at 16,000 × *g* for 1 min. The supernatant containing the unabsorbed phage
282 was then spotted in three technical replicates on double-layered agar containing either *K.*
283 *pneumoniae* MKP103 or *K. pneumoniae* MKP103 (p_{Vector}); strains carrying the plasmid (empty
284 vector and complemented) were plated with *K. pneumoniae* MKP103 (p_{Vector}). Plaques were
285 enumerated following overnight incubation at 37°C. Three biological replicates were
286 conducted for each group.
287
288 *Fluorescent and confocal microscopic assay*
289 Phage pKMKP103_1 was incubated with 100× SYBR™ Gold Nucleic Acid stain
290 (Invitrogen™) at 4°C for 4 h. The stained pKMKP103_1 was then transferred to an Amicon®
291 Ultra-15 centrifugal filter tube (MWCO 100 kDa) and centrifuged at 3,220 × *g* and 4°C to
292 remove excess stain. Two further washes with SM buffer were conducted prior to
293 resuspension of the stained pKMKP103_1 in an equal volume of SM buffer. Enumeration of

294 the plaques was performed to determine the titer of stained pKMKP103_1 for the microscopic
295 assays. The log-phase bacterial culture was grown and diluted to 2×10^7 cfu/mL, and
296 incubated with FM™ 4-64FX membrane stain (Invitrogen™) at room temperature for 5 min.
297 The SYBR™ Gold stained pKMKP103_1 was added to the FM™ 4-64FX stained *K. pneumoniae*
298 at an MOI of 100 (fluorescent microscopy) and 1,000 (confocal microscopy). For fluorescent
299 microscopy, the mixture was applied directly onto the glass slide. For confocal microscopy,
300 the mixture was mixed with molten 2% agarose (55°C) to fix the sample for imaging.
301
302 *One-step growth curve*
303 Log-phase *K. pneumoniae* culture was diluted to ~10^7 cfu/mL and phage pKMKP103_1
304 added to achieve a final titer of 10^5 pfu/mL (MOI 0.01). Following 2-min incubation at 37°C
305 the culture was centrifuged at 16,000 × *g* for 1 min, the supernatant containing the free phage
306 was removed and the bacterial pellet was resuspended in an equal volume of nutrient broth.
307 Aliquots (100 µL) were then removed at 10-min intervals and added to a glass tube containing
308 4 mL soft agar with 100 µL bacterial culture of *K. pneumoniae* MKP103 or *K. pneumoniae*
309 MKP103 (p_{Vector}). Following a rapid vortex, the entire content of the tube was poured onto a
310 nutrient agar plate to form a double-layered agar. Plaques were enumerated following
311 overnight incubation at 37°C.
312
313 *Mutation frequency to pKMKP103_1*
314 The mutation frequency of *K. pneumoniae* strains to pKMKP103_1 was examined
315 using the agar overlay method[46] with modifications. *K. pneumoniae* was grown to log-phase
316 as described above to an OD_{600nm} of 0.5 (equivalent to ~10^8 cfu/mL). For mutants carrying the
317 empty vector and complemented strains, 5 mg/L gentamicin was added as the selection

318 pressure to maintain the plasmid. Bacterial culture was centrifuged at 16,000 × *g* at 4°C and
319 the pellet was resuspended in an equal volume of 0.9% NaCl. The bacterial culture was serially
320 diluted and 100 µL was added to a glass tube containing 4 mL soft agar with pKMKP103_1
321 (10^9 pfu/mL). Control samples without phage were included to obtain the total number of
322 colonies. A double-layered agar was prepared as described above. Colonies were counted
323 following a 20-h incubation at 37°C. Mutation frequency was calculated by dividing the
324 number of colonies formed on the agar containing pKMKP103_1 over the total number of
325 colonies. Statistical analysis was conducted using the multiple comparisons with uncorrected
326 Dunn's test on GraphPad Prism 9.3.1.
327
328 *Antibiotic susceptibility testing and population analysis profiles (PAPs)*
329 Susceptibility of *K. pneumoniae* strains to a range of antibiotics was determined using
330 broth microdilution (Trek Sensititre®, ThermoFisher Scientific) as per the manufacturer's
331 instructions. The lowest antibiotic concentration that inhibited the visible growth of bacteria
332 was the MIC. For mutants that showed a 2-fold difference in MIC compared to the WT strain
333 and demonstrated restoration of the MIC following complementation (**Supplementary Table**
334 **2**), additional broth microdilution assays were conducted in two technical replicates and
335 confirmed on two separate occasions. All MIC assays were conducted in cation-adjusted (22.5
336 mg/L Ca^{2+}, 11.25 mg/L Mg^{2+}) Mueller Hinton broth (CAMHB).
337 PAPs were undertaken as described previously with minor modifications[47]. Briefly,
338 bacterial culture was grown in CAMHB until log-phase and following 10-fold serial dilutions,
339 cultures were plated onto MH agar containing colistin at 2, 4, 8, 16, 32, 64 or 128 mg/L. Viable
340 colonies were enumerated following overnight incubation at 37°C.
341

342 *Lipid A profiling*

343 A single bacterial colony was inoculated in CAMHB and incubated at 37°C with shaking
344 (200 rpm) for 18 h. The overnight culture was then diluted 1:100 with fresh CAMHB (final
345 volume, 200 mL) and grown to an OD_{600nm} of ~0.7 (8.35±0.13 log_{10} cfu/mL). Bacterial pellets
346 were collected via centrifugation at 9,000 × *g* for 10 min, washed twice with 0.9% NaCl, and
347 resuspended in 4 mL of 0.9% NaCl. Lipid A extraction was conducted with minor
348 modifications[48]. Methanol (10 mL) and chloroform (5 mL) were then added to prepare a
349 single-phase Bligh-Dyer mixture (chloroform:methanol:water, 1:2:0.8, v/v) for the extraction
350 of LPS. LPS pellet was obtained by centrifugation at 3,220 × *g* for 10 min and washed once
351 with single-phase Bligh-Dyer mixture. The washed pellet was resuspended in 5.4 mL of
352 hydrolysis buffer (50 mM sodium acetate, pH 4.5) and incubated in a boiling water bath for 1
353 h. Following hydrolysis, methanol (6 mL) and chloroform (6 mL) was added to make a two-
354 phase Bligh-Dyer mixture (chloroform:methanol:water, 1:1:0.9, v/v). Following centrifugation
355 at 3,220 × *g* for 10 min, the lower phase of the mixture containing the lipid A was collected,
356 dried and stored at -20°C. Prior to LC-MS analysis, the dried lipid A was resuspended in 200
357 µL of chloroform:methanol (1:1, v/v), centrifuged at 14,000 × *g* for 10 min, and 150 µL of
358 supernatant was collected. An equal volume of isopropanol:water (2:1, v/v) was then added
359 prior to centrifugation at 14,000 × *g* for 10 min, and 200 µL of supernatant was obtained for
360 LC-MS analysis on the Dionex U3000 high-performance liquid chromatography (HPLC) system
361 in tandem with a Q-Exactive Orbitrap high-resolution mass spectrometer (Thermo Fisher).
362

Acknowledgements

We would like to express our gratitude to the Ramaciotti Centre for Cryo-Electron Microscopy (Monash University) and Micromon Genomics (Monash University) for their facilities to conduct TEM imaging and Sanger sequencing. This study was supported by the National Institute of Allergy and Infectious Diseases of the National Institutes of Health (R21 AI156766) and a Monash-UCSD Seed Fund. J.L. is an NHMRC Principal Research Fellow (APP1157909). The content is solely the responsibility of the authors and does not necessarily represent the official views of the National Institute of Allergy and Infectious Diseases or the National Institutes of Health.

Contributions

S.C.N. and J.L. conceived the study. D.T.M provided the sewage sample for phage isolation. S.C.N, J.L., H.H.Y., H.W., M.A.K.A, M.H., J.Z., N.S., B.P.H and Y.Z. conducted the experiments. S.C.N, P.J.B. T.V. and J.L. wrote and edited the manuscript. G.R., T.V., S.A., R.T.S., J.J.B and J.L. supervised and funded the project. All authors reviewed and agreed to the final manuscript.

References

1. Taylor MW. *Viruses and man: A history of interactions*. Springer, Cham (2014).

2. Campbell A. The future of bacteriophage biology. *Nat Rev Genet* **4**, 471-477 (2003).

3. Lin DM, Koskella B, Lin HC. Phage therapy: An alternative to antibiotics in the age of multi-drug resistance. *World J Gastrointest Pharmacol Ther* **8**, 162-173 (2017).

4. Brives C, Pourraz J. Phage therapy as a potential solution in the fight against AMR: Obstacles and possible futures. *Palgrave Commun* **6**, 100 (2020).

5. Chanishvili N. Phage therapy--history from Twort and d'Herelle through Soviet experience to current approaches. *Adv Virus Res* **83**, 3-40 (2012).

6. Fleming A. Classics in infectious diseases: On the antibacterial action of cultures of a penicillium, with special reference to their use in the isolation of *B. influenzae* by Alexander Fleming, Reprinted from the British Journal of Experimental Pathology 10:226-236, 1929. *Rev Infect Dis* **2**, 129-139 (1980).

7. Butler MS, Blaskovich MA, Cooper MA. Antibiotics in the clinical pipeline at the end of 2015. *J Antibiot (Tokyo)* **70**, 3-24 (2017).

8. Rossolini GM, Arena F, Pecile P, Pollini S. Update on the antibiotic resistance crisis. *Curr Opin Pharmacol* **18**, 56-60 (2014).

9. Antimicrobial Resistance Collaborators. Global burden of bacterial antimicrobial resistance in 2019: A systematic analysis. *Lancet* **399**, 629-655 (2022).

10. Rice LB. Federal funding for the study of antimicrobial resistance in nosocomial pathogens: no ESKAPE. *J Infect Dis* **197**, 1079-1081 (2008).

11. World Health Organization. Antibiotic resistance. https://www.who.int/news-room/fact-sheets/detail/antibiotic-resistance (2020).

12. Centers for Disease Control and Prevention. Antibiotic/Antimicrobial resistance (AR/AMR). https://www.cdc.gov/drugresistance/index.html (2021).

13. Kortright KE, Chan BK, Koff JL, Turner PE. Phage therapy: A renewed approach to combat antibiotic-resistant bacteria. *Cell Host Microbe* **25**, 219-232 (2019).

14. Gurney J*, et al.* Phage steering of antibiotic-resistance evolution in the bacterial pathogen, *Pseudomonas aeruginosa*. *Evol Med Public Health* **2020**, 148-157 (2020).

15. Gordillo Altamirano F*, et al.* Bacteriophage-resistant *Acinetobacter baumannii* are resensitized to antimicrobials. *Nat Microbiol* **6**, 157-161 (2021).

424 16. Hesse S*, et al.* Phage resistance in multidrug-resistant *Klebsiella pneumoniae* ST258
425 evolves via diverse mutations that culminate in impaired adsorption. *mBio* **11**,
426 e02530-02519 (2020).
427
428 17. Burmeister AR*, et al.* Pleiotropy complicates a trade-off between phage resistance and
429 antibiotic resistance. *Proc Natl Acad Sci U S A* **117**, 11207-11216 (2020).
430
431 18. Li P, Lin H, Mi Z, Xing S, Tong Y, Wang J. Screening of polyvalent phage-resistant
432 *Escherichia coli* strains based on phage receptor analysis. *Front Microbiol* **10**, 850
433 (2019).
434
435 19. Ramage B*, et al.* Comprehensive arrayed transposon mutant library of *Klebsiella*
436 *pneumoniae* outbreak strain KPNIH1. *J Bacteriol* **199**, e00352-00317 (2017).
437
438 20. Alikhan NF, Petty NK, Ben Zakour NL, Beatson SA. BLAST Ring Image Genarator (BRIG):
439 Simple prokaryote genome comparisons. *BMC Genomics* **12**, 402 (2011).
440
441 21. Killmann H, Videnov G, Jung G, Schwarz H, Braun V. Identification of receptor binding
442 sites by competitive peptide mapping: phages T1, T5, and phi 80 and colicin M bind to
443 the gating loop of FhuA. *J Bacteriol* **177**, 694-698 (1995).
444
445 22. Killmann H, Braun V. Energy-dependent receptor activities of *Escherichia coli* K-12:
446 mutated TonB proteins alter FhuA receptor activities to phages T5, T1, ⊘80 and to
447 colicin M. *FEMS Microbiol Lett* **119**, 71-76 (1994).
448
449 23. Langenscheid J, Killmann H, Braun V. A FhuA mutant of *Escherichia coli* is infected by
450 phage T1-independent of TonB. *FEMS Microbiol Lett* **234**, 133-137 (2004).
451
452 24. Armengod ME*, et al.* Enzymology of tRNA modification in the bacterial MnmEG
453 pathway. *Biochimie* **94**, 1510-1520 (2012).
454
455 25. Liu X*, et al.* Involvement of RpoN in regulating motility, biofilm, resistance, and
456 spoilage potential of *Pseudomonas fluorescens*. *Front Microbiol* **12**, 641844 (2021).
457
458 26. Mahmud A*, et al.* Genome-scale mapping reveals complex regulatory activities of
459 RpoN in *Yersinia pseudotuberculosis*. *mSystems* **5**, e01006-01020 (2020).
460
461 27. Leang C*, et al.* Genome-wide analysis of the RpoN regulon in *Geobacter sulfurreducens*.
462 *BMC Genomics* **10**, 331 (2009).
463
464 28. Burgess RR. *Encyclopedia of genetics: Sigma factors*. Academic Press (2001).
465
466 29. Wright RCT, Friman VP, Smith MCM, Brockhurst MA. Cross-resistance is modular in
467 bacteria-phage interactions. *PLoS Biol* **16**, e2006057 (2018).
468
469 30. Lloyd MG*, et al.* Targeting the alternative sigma factor RpoN to combat virulence in
470 *Pseudomonas aeruginosa*. *Sci Rep* **7**, 12615 (2017).

31. Prunier AL, Leclercq R. Role of *mutS* and *mutL* genes in hypermutability and recombination in *Staphylococcus aureus*. *J Bacteriol* **187**, 3455-3464 (2005).

32. Willems RJ, Top J, Smith DJ, Roper DI, North SE, Woodford N. Mutations in the DNA mismatch repair proteins MutS and MutL of oxazolidinone-resistant or -susceptible *Enterococcus faecium*. *Antimicrob Agents Chemother* **47**, 3061-3066 (2003).

33. Oliver A, Baquero F, Blázquez J. The mismatch repair system (*mutS*, *mutL* and *uvrD* genes) in *Pseudomonas aeruginosa*: Molecular characterization of naturally occurring mutants. *Mol Microbiol* **43**, 1641-1650 (2002).

34. Galán JC*, et al.* Mutation rate is reduced by increased dosage of *mutL* gene in *Escherichia coli* K-12. *FEMS Microbiol Lett* **275**, 263-269 (2007).

35. Woodford N, Ellington MJ. The emergence of antibiotic resistance by mutation. *Clin Infect Dis* **13**, 5-18 (2007).

36. Shen M*, et al. Pseudomonas aeruginosa* MutL promotes large chromosomal deletions through non-homologous end joining to prevent bacteriophage predation. *Nucleic Acids Res* **46**, 4505-4514 (2018).

37. Majkowska-Skrobek G, Markwitz P, Sosnowska E, Lood C, Lavigne R, Drulis-Kawa Z. The evolutionary trade-offs in phage-resistant *Klebsiella pneumoniae* entail cross-phage sensitization and loss of multidrug resistance. *Environ Microbiol* **23**, 7723-7740 (2021).

38. Bonilla N, Rojas MI, Netto Flores Cruz G, Hung SH, Rohwer F, Barr JJ. Phage on tap-a quick and efficient protocol for the preparation of bacteriophage laboratory stocks. *PeerJ* **4**, e2261 (2016).

39. Dunstan RA*, et al.* The flagellotropic bacteriophage YSD1 targets *Salmonella* Typhi with a Chi-like protein tail fibre. *Mol Microbiol* **112**, 1831-1846 (2019).

40. Prjibelski A, Antipov D, Meleshko D, Lapidus A, Korobeynikov A. Using SPAdes de novo assembler. *Curr Protoc Bioinformatics* **70**, e102 (2020).

41. McNair K, Aziz RK, Pusch GD, Overbeek R, Dutilh BE, Edwards R. Phage genome annotation using the RAST pipeline. *Methods Mol Biol* **1681**, 231-238 (2018).

42. Arndt D*, et al.* PHASTER: A better, faster version of the PHAST phage search tool. *Nucleic Acids Res* **44**, W16-W21 (2016).

43. Thung TY*, et al.* Component parts of bacteriophage virions accurately defined by a machine-learning approach built on evolutionary features. *mSystems* **6**, e0024221 (2021).

518 44. Kovach ME*, et al.* Four new derivatives of the broad-host-range cloning vector
519 pBBR1MCS, carrying different antibiotic-resistance cassettes. *Gene* **166**, 175-176
520 (1995).
521
522 45. Kutter E. Phage host range and efficiency of plating. *Methods Mol Biol* **501**, 141-149
523 (2009).
524
525 46. Blasco L*, et al.* Combined use of the Ab105-2ϕΔCI lytic mutant phage and different
526 antibiotics in clinical isolates of multi-resistant *Acinetobacter baumannii*.
527 *Microorganisms* **7**, 556 (2019).
528
529 47. Li J*, et al.* Heteroresistance to colistin in multidrug-resistant *Acinetobacter baumannii*.
530 *Antimicrob Agents Chemother* **50**, 2946-2950 (2006).
531
532 48. Henderson JC, O'Brien JP, Brodbelt JS, Trent MS. Isolation and chemical
533 characterization of lipid A from Gram-negative bacteria. *J Vis Exp*, e50623 (2013).
534
535

536

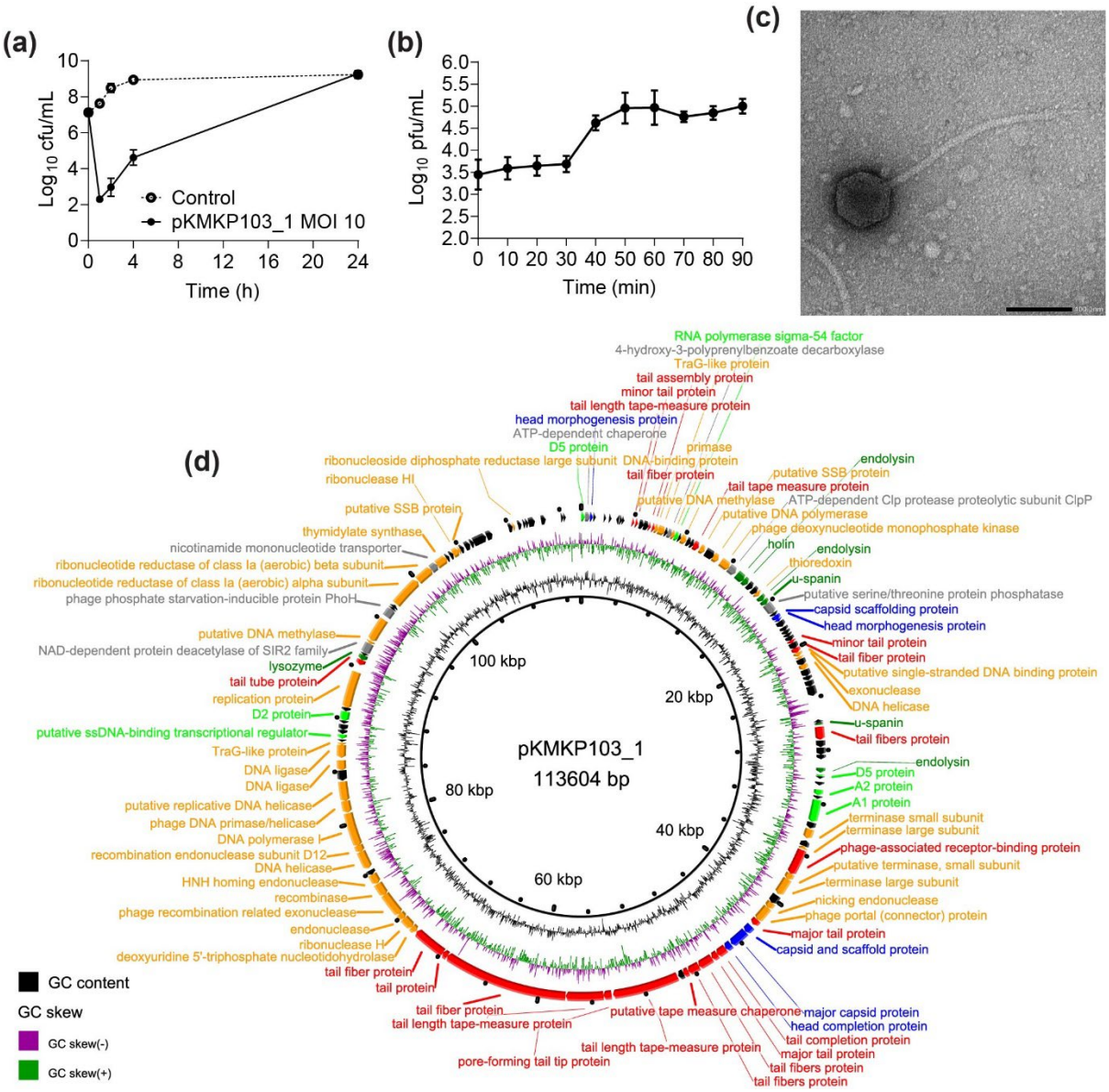

537

538 **Figure 1.** Basic characterization of phage pKMKP103_1. **(a)** Time-kill kinetics of phage
539 pKMKP103_1 against *K. pneumoniae* MKP103 at an MOI of 10 (*n*=3). **(b)** One-step growth
540 curve of pKMKP103_1 with *K. pneumoniae* MKP103 (*n*=3). **(c)** A representative TEM image of
541 pKMKP103_1. The scale bar represents 100 nm. **(d)** The pKMKP103_1 genome visualized
542 using BRIG[20]. The colors represent the functions of the genes: orange (DNA packaging,
543 replication, and modification), lime (transcription), green (host lysis), blue (head structural
544 components), red (tail structural components), gray (others/unknown functions), and black
545 (hypothetical).

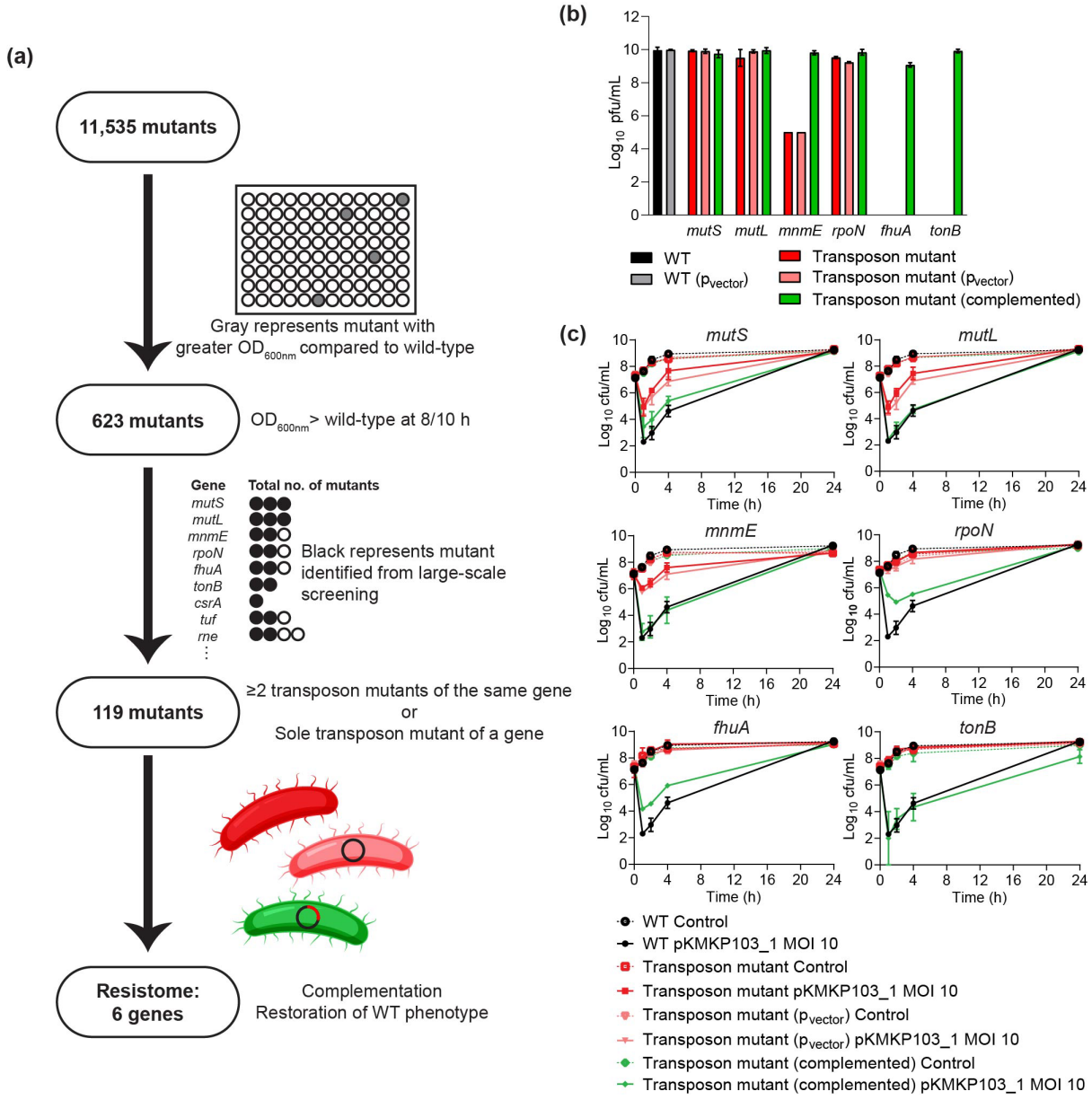

Figure 2. Identification of *K. pneumoniae* MKP103 genes that are correlated with phage pKMKP103_1 resistance and the associated resistance phenotype. **(a)** Workflow for the genome-wide transposon screening of pKMKP103_1 resistome using the transposon mutant library. **(b)** The plaque forming unit (pfu) when pKMKP103_1 was plated on the respective *K. pneumoniae* MKP103 strains. Individual plaque counts were not available for *mnmE*::Tn and *mnmE*::Tn (p_{vector}); the count was calculated based on the highest dilution in which lysis zone could be observed. Data are presented as mean ± s.d. (*n*=3). **(c)** Time-kill kinetics of pKMKP103_1 against *K. pneumoniae* MKP103 and mutant strains at an MOI of 10 (*n*=3).

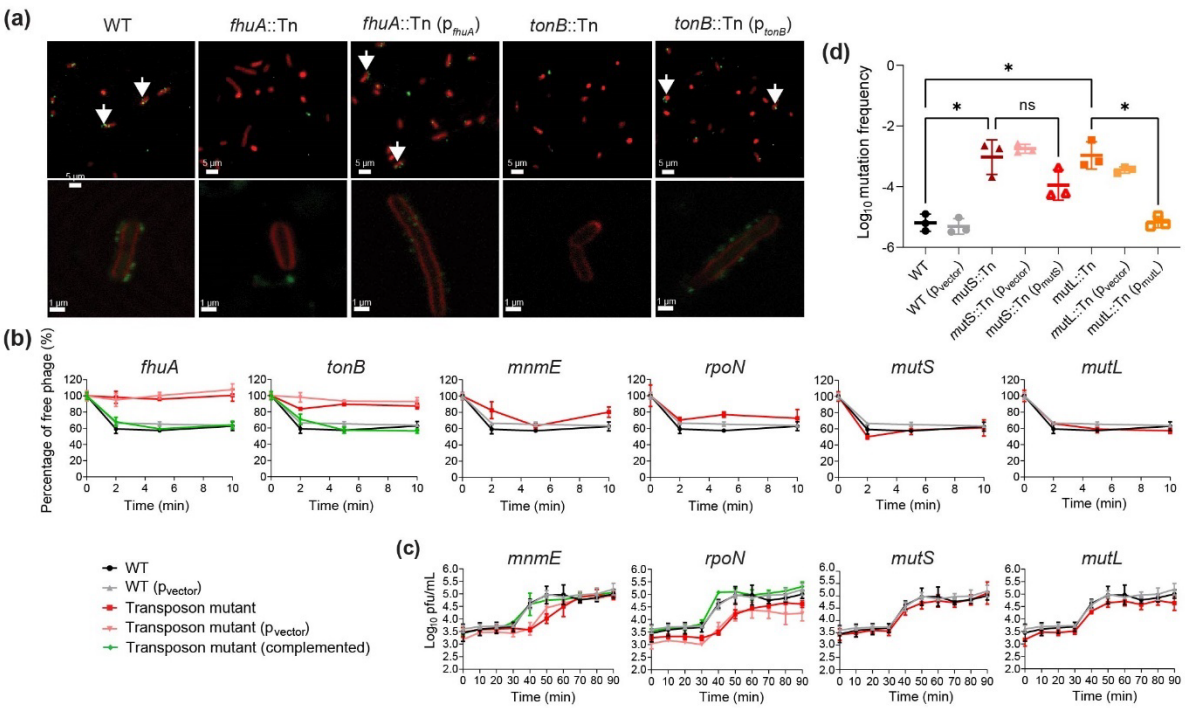

Figure 3. Phage pKMKP103_1 adsorption, one-step growth profiles and bacterial mutation frequency towards pKMKP103_1. **(a)** Visualization of pKMKP103_1 adsorption determined using fluorescent (top panels) and confocal (bottom panels) microscopy. The pKMKP103_1 was stained with SYBR™ Gold strain (green) and *K. pneumoniae* MKP103 strains were stained with FM™ 4-64FX (red). **(b)** pKMKP103_1 adsorption profile with respective *K. pneumoniae* strains (n=3). **(c)** One-step growth profile of pKMKP103_1 in the presence of different *K. pneumoniae* strains. Data is presented as the mean ± s.d. (n=3). **(d)** The mutation frequency of *K. pneumoniae* strains to phage pKMKP103_1 (n=3). Statistical significance is denoted with *p<0.05.

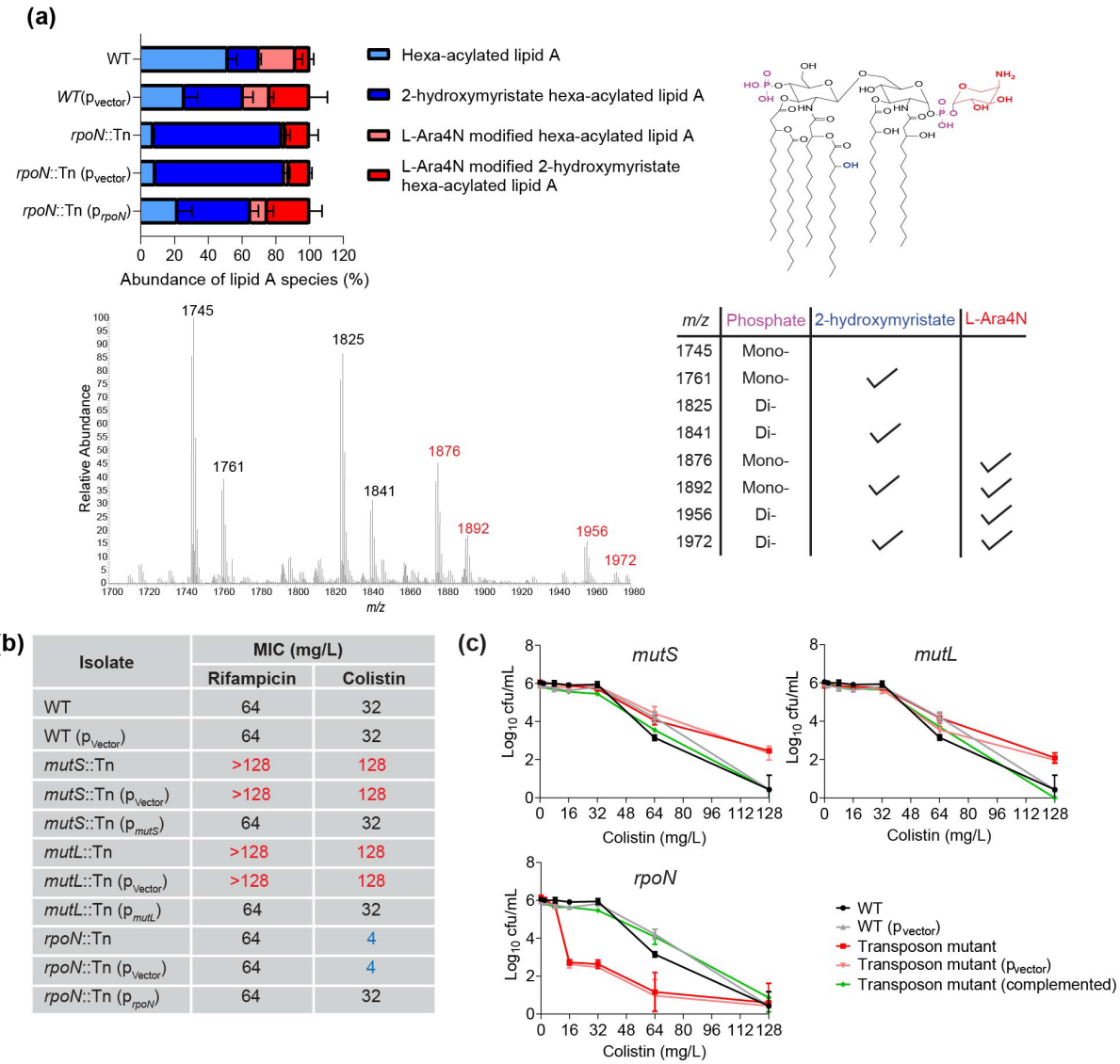

Isolate	MIC (mg/L)	
	Rifampicin	Colistin
WT	64	32
WT (p_{Vector})	64	32
mutS::Tn	>128	128
mutS::Tn (p_{Vector})	>128	128
mutS::Tn (p_{mutS})	64	32
mutL::Tn	>128	128
mutL::Tn (p_{Vector})	>128	128
mutL::Tn (p_{mutL})	64	32
rpoN::Tn	64	4
rpoN::Tn (p_{Vector})	64	4
rpoN::Tn (p_{rpoN})	64	32

Figure 4. Lipid A and antibiotic susceptibility profiles. **(a)** Analysis of the individual lipid A species abundance in relative to the total abundance (*n*=3). Representative mass spectrum profile and chemical structure of each lipid A species. **(b)** Minimum inhibitory concentrations (MICs) of rifampicin and colistin. Increased and decreased MICs compared to *K. pneumoniae* MKP103 (WT) were represented by red and blue font colors, respectively. **(c)** Population analysis profiles of *K. pneumoniae* strains on MH agar containing colistin at 2, 4, 8, 16, 32, 64 and 128 mg/L (*n*=3).

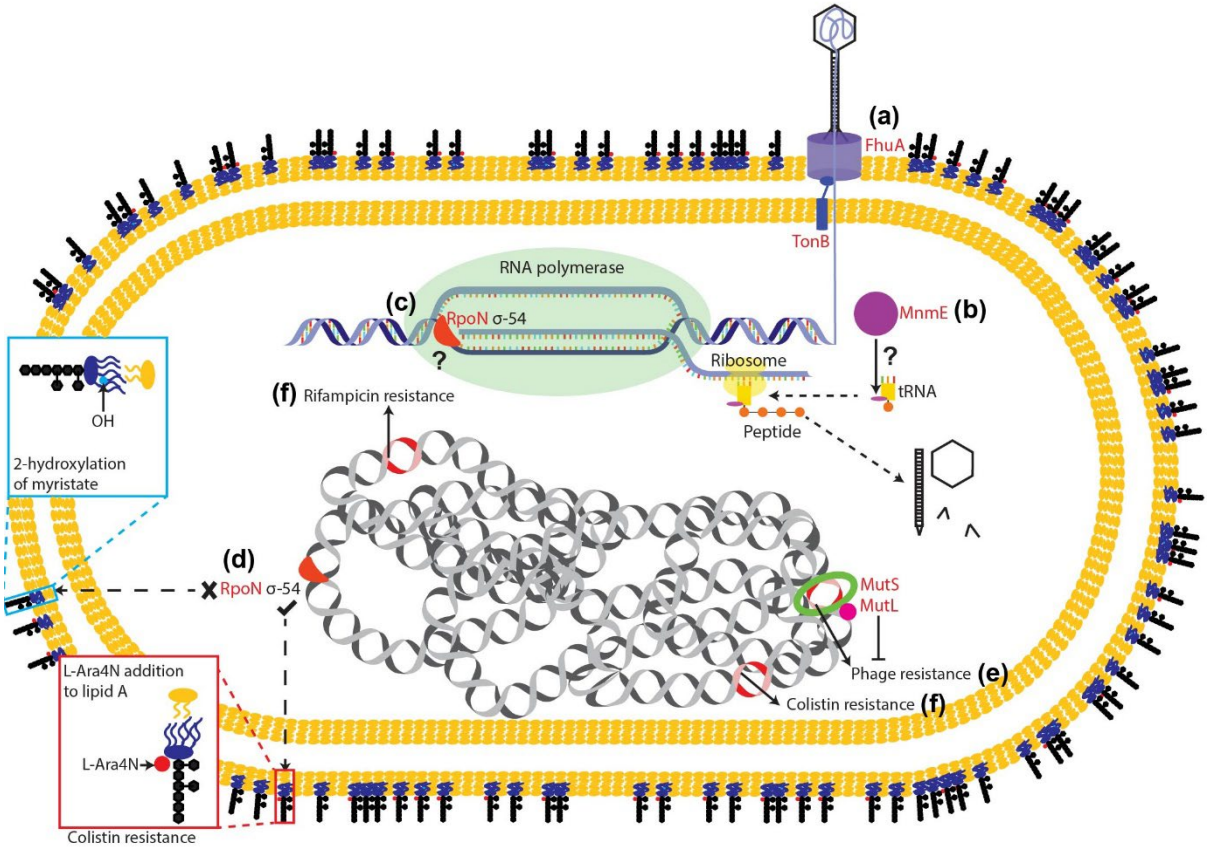

Figure 5. Schematic diagram representing the proposed mechanisms of phage resistance in *K. pneumoniae* MKP103, and the interrelationships with rifampicin and colistin resistance. **(a)** A TonB-dependent FhuA is required for the adsorption of phage. **(b)** MnmE potentially involves in the modification of tRNA, enhancing the protein synthesis for phage particles. **(c)** RpoN could affect the transcription of the phage genome. **(d)** RpoN regulates bacterial transcription for cationic lipid A modifications that confer colistin resistance. MutS and MutL mediate DNA mismatch repair prevent chromosomal mutations associated with resistance to **(e)** phage, **(f)** rifampicin and colistin.